Ocean Variability Effects on High-Frequency Acoustic Propagation in KauaiEx

Mohsen Badiey[1], Stephen E. Forsythe[2], Michael B. Porter[3], and the KauaiEx Group

[1]*College of Marine Studies, University of Delaware, Newark, DE 19716*
[2]*Naval Undersea Warfare Center, Newport, RI, 02841*
[3]*Science Applications International, San Diego, CA 92121*

Abstract. During the Kauai experiment in summer of 2003 a bottom-mounted vertical line array containing 8 hydrophones spaced 0.6 meter apart was deployed in a 100-m shallow water region near the Pacific Missile Range Facility. The acoustic source was placed about 2 km away on a flat sea bottom at 95 meter water depth. The element spacing was sufficiently small to allow measurements of the temporal variability of time-angle intensity fluctuations of the acoustic energy. Measurements were made simultaneously of the broadband acoustic pulse transmissions (8-50 kHz) and environmental parameters. The latter measurements included current, temperature and salinity profiles, directional surface wave spectra, as well as wind speed and direction above the sea surface. Arrival time-angle fluctuations were found to be correlated with the environmental variability due to ocean dynamics in this region. It is shown that variations of the sea surface dynamics exhibit different temporal effects than those occurring within the water column.

INTRODUCTION

Variability of ocean physical parameters can cause significant fluctuations in the arrival of broadband acoustic signals in shallow water. Arrival time and angle information of a pulse is a useful quantity in different applications of underwater acoustics because it can be a good indicator of the dynamics of the ocean volume or boundaries. The arrival time of energy following a particular ray path depends on sound speed and current of the ocean through which the ray passes and on roughness of the ocean boundaries with which reflects or scatters.

In shallow water, where the energy traveling along several ray paths may contribute to an arriving signal, significant signal bandwidth is necessary to distinguish (temporally) the arrivals corresponding to individual ray paths. Even with sufficient signal bandwidth, on a windy day having a rough sea surface it may be difficult to identify an arrival time for an individual ray that intersects the sea surface, due to the time and angle spreading and collective interference of the scattered energy. To address these issues a highly calibrated acoustic experiment was conducted during the summer 2003 at a shallow water location near the Kauai Island, Hawaii.

The Kauai Experiment (KauaiEx) was conducted from June 22 to July 9, 2003 with the objective to study high-frequency (8-50 kHz) acoustic propagation in a shallow water waveguide. In contrast to much of the previous literature, emphasis was placed on multipath arising from multiple boundary interactions. The main theme of this experiment was the role of the environmental physical parameters on high-frequency acoustic signals applicable to underwater communications. A great deal of effort was made to characterize the environment including the surface wave spectrum, 2-D temperature structure along the propagation path, salinity, currents, and bottom properties. Using autonomous instruments, most of these parameters were measured continuously over the two weeks of the experiment providing information on the diurnal cycles. At the same time, extensive acoustic measurements were made using a variety of vertical line arrays some of which spanned the entire water column. Detailed description of the experiment and the overview is provided in [1]. During the course of the experiment there were actually three different deployments of acoustic source and receiver arrays. In this paper, the results are presented from the second deployment pertaining to a fixed vertical line array placed on the sea floor 2 km from the acoustic source. A brief description of the oceanographic data is presented followed by the acoustic measurements and data analysis.

MEASUREMENTS

Oceanographic Measurements

Detailed oceanographic measurements made during the experiment included directional surface waves, water column temperature and salinity profiles at different points along a 6-km propagation path. The current profile, wind speed and direction were also measured at single points. Figure 1 shows the schematic diagram of the acoustic and the environmental measurement arrays. The sea surface waves and temperature profile near the bottom mounted receiver array for a period of 47 hours (from 11:00 AM July 1 through 10:00 AM July 3, 2003) are presented here. During this time the temporal variability of acoustic signals is shown to be correlated with the environmental variability.

Five thermistor arrays were placed along the propagation track to measure temporal and spatial distribution of the sound speed during the experiment. Measurements of the salinity profile at different points showed a negligible variation. Therefore, the salinity is considered constant for calculation of the sound speed profile. For data discussed here, the temperature profile (UDEL Themistor String in Fig. 1) near the receiver array at 2 km from the sound source is shown in Fig. 2. This time corresponds to the same time for which both surface waves and the acoustic propagation measurements were made.
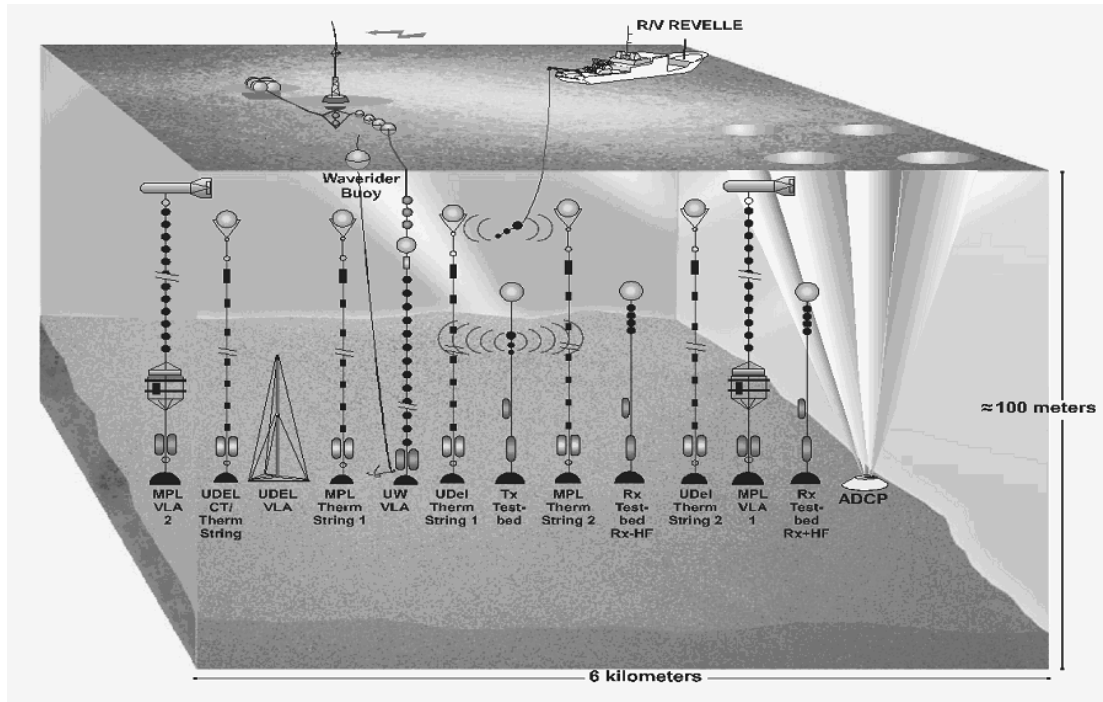
FIGURE 1: Schematic diagram of the Kauai Experiment. Data from UDEL Vertical Line Array (VLA) and UDEL-CT Thermistor String are discussed here.

It is noticed that for most of this time the water column is a very well mixed layer down to about 50 m depth. A cold layer (about 4-5 degrees C lower than the mixed layer) emerges at nearly tidal cycles. Variations of this layer pertaining to oceanographic features are repeated during the entire experiment.

Hourly measurements of wave frequency spectra were made during the entire experiment using a directional buoy. The wave spectrum and the wind speed for the period from 11:00 AM July 1 through 10:00 AM July 3, 2003 are shown in Fig. 3. The right plot shows hourly measurements of the non-directional wave frequency spectra. These plots show that changes in spectral level correspond to changes in wind speed. Changes in high-frequency spectral levels are abrupt while changes in low frequency spectral levels occur gradually. It is noticed that surface wave energy changes in three different distinct frequency bands. Open ocean swells show up on (0.05 – 0.1 Hz) which are low frequency waves traveling in from the open ocean from far distances. Then the wind generated surface waves arrive at two different bands. First, there are larger scale waves formed after the wind has blown in the same direction for some duration of time (0.1 -0.2 Hz), and then small scale surface chop (0.2-0.35 Hz) that appears almost immediately after wind speed increases and disappears shortly after wind speed decreases or changes direction (this is referred to as the land breeze effect).
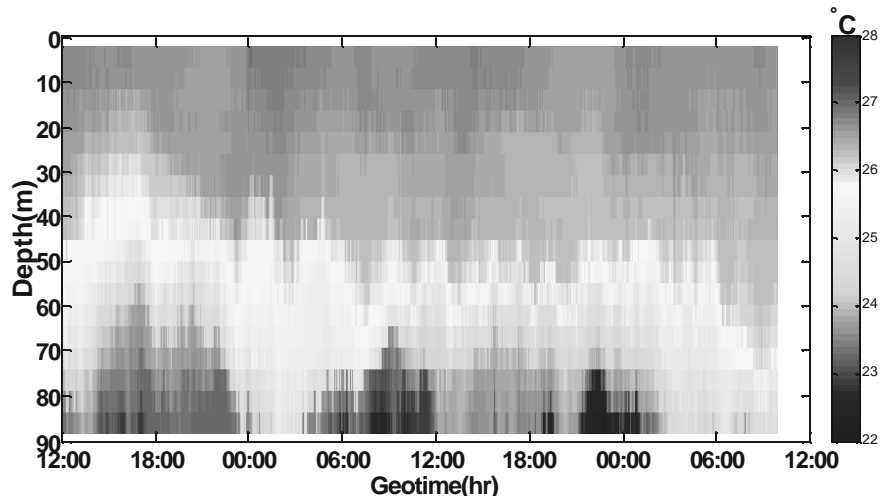
FIGURE 2: Temperature profile for the UDEL-CT/Thermistor String mooring from 11:00 AM on July 1 through 10:00 AM on July 3, 2003.

Changes in spectral levels for the 0.2 – 0.3 Hz small scale, surface-chop frequency show an immediate increase and decrease corresponding to changes in wind speed. Spectral levels for the 0.1 - 0.2 Hz larger scale wind-generated waves show the same correspondence to changes in wind speed, but spectral level changes occur on longer time scales. Energy remains in this frequency band for sometime after wind speeds decrease.

For both days covered in this period, wind speeds undergo a late morning increase and a late night decrease. Changes in spectral levels for the 0.2 – 0.3 Hz small scale, surface-chop frequency show an immediate increase and decrease corresponding to changes in wind speed. Spectral levels for the 0.1 - 0.2 Hz larger-scale wind generated waves show the same correspondence to changes in wind speed, but spectral level changes occur on longer time scales. Energy remains in this frequency band for some time after wind speeds decrease and generally the dominant wave direction corresponds to wind direction. This indicates the majority surface wave energy is coming from wind-generated waves.

In an acoustic measurement the sea-surface fluctuations may induce fast fluctuations in the acoustic signal propagation while temporal variability of the sound speed profile may induce large-scale fluctuations. To resolve both these scales, we consider different sampling of the ocean on both short and long geophysical time scales.
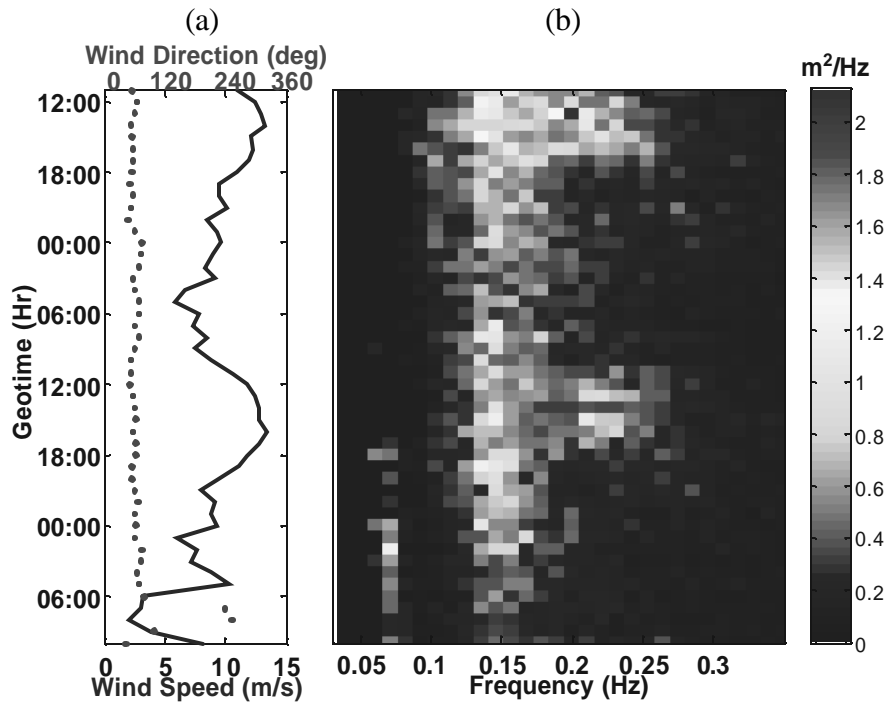
FIGURE 3: (a) Hourly wind speed and direction; (b) Measured sea surface wave frequency data from 11:00 AM July 1 through 10:00 AM July 3. This period corresponds to 48 hours of acoustic data recorded on the bottom mounted vertical acoustic line array.

ACOUSTIC MEASUREMENTS

A set of four LFM sweeps with variable duration was transmitted in three frequency bands (low 8-16 kHz, mid 14-22 kHz, and high 25-50 kHz). The duration of these chirp signals was 40, 80, 160 and 320 milliseconds (msec.) respectively. These four sweeps were transmitted nine times with a 3-second time interval in between transmissions, for a total duration of 27 seconds. This group of nine transmissions is used to estimate variability over a short time scale. Groups of nine were transmitted with the time interval of 30 minutes throughout the experiment period. The variable durations are designed to help characterize surface variability over a very short time scale by providing different times over which to average the surface reflected signals. In this paper we describe the signals transmitted in the 8-16 kHz frequency band. The impulse response for the water column shown in Fig. 4 is obtained by correlating the arrivals at the receiver array with the original transmitted signal.
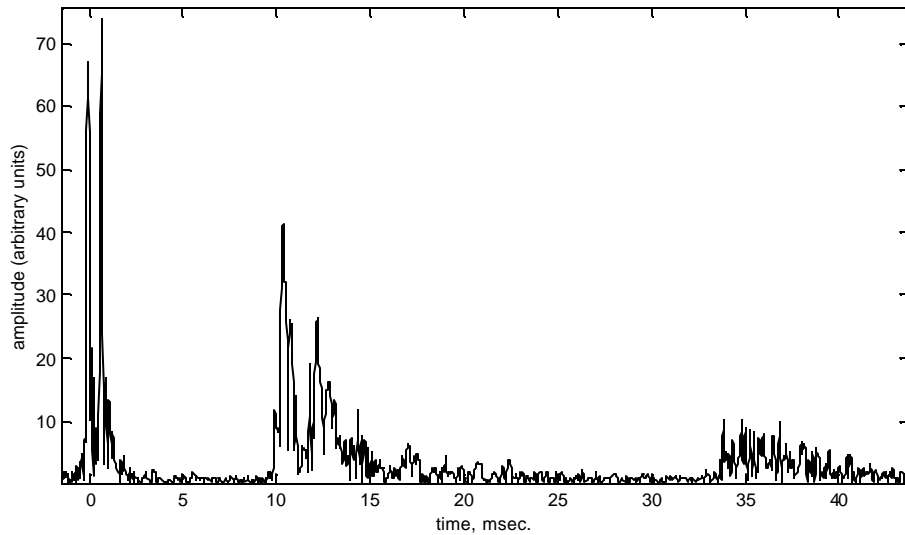
FIGURE 4 - Matched-filtered signal for a typical pulse arrival for geotime 7/2/04 12:31 PM.

The distinct early arrivals (around 0 msec.), which are bottom interacting, are subject to one or more bottom bounces. Surface-interacting ray groups arrive starting at around 10 and 34 msec. Since the original transmitted signal is broadband (8-16 kHz), sub-bands of the signal can be used to provide a time-averaged value of the arrivals. Here a 2 kHz bandwidth has been used to give a resolution of about 0.5 msec. for 3 dB down from max peak.

The 8-hydrophone receiver array mounted in a vertical stave has roughly a 4 m aperture. This array is used in a beamforming algorithm designed to provide better resolution of the ray arrivals by showing the acoustic field arrival in both time and angle. Beams are formed by taking the Fourier transform of the 8 channels' digitized time series and multiplying each channel by a complex phasor to "correct" the expected phase shift (as a function of frequency and arrival angle) between the vertically-deployed hydrophones in the array. The 8 corrected Fourier transforms are then summed and the inverse Fourier transform applied to give a single time series. This signal is effectively spatially filtered to look only at the incoming energy from the selected arrival angle. The process is repeated for all arrival angles between -20 and 20 degrees. The envelope is then formed using a Hilbert-transform, and displayed as a false-color image in Fig. 5. The correction formula is $\phi_{ij} = k_i z_j \sin\theta = \dfrac{2\pi f_i}{c} z_j \sin\theta$,

where ϕ_{ij} is the phase correction to the ith spectral amplitude of the jth channel of the 8 hydrophones' time series, z_j is the vertical displacement of the jth hydrophone from the center of the array, and θ is the selected angular direction for the spatial filtering operation. While the element spacing was fairly small, it was not sufficiently small to eliminate grating-lobe effects that appear as repeating patterns in the angular direction of the time-angle plot. As an example, energy arriving from 0 degrees (horizontal) needs no phase correction, since $\sin\theta = 0$ for that angle. However, if the product,

$\frac{f}{c}\Delta z \sin \boldsymbol{q}$, (where Δz is the spacing between adjacent elements) is equal to 1, the phase shift is also 0, which is indistinguishable from the horizontally incident case. So, the angle at which aliased energy arrives horizontally is $\boldsymbol{q} = \sin^{-1}\left(\frac{c}{f\Delta z}\right)$. A sample time-angle plot for a pulse transmission during July 1, 2003 at 12:31 PM is shown in Fig. 5.
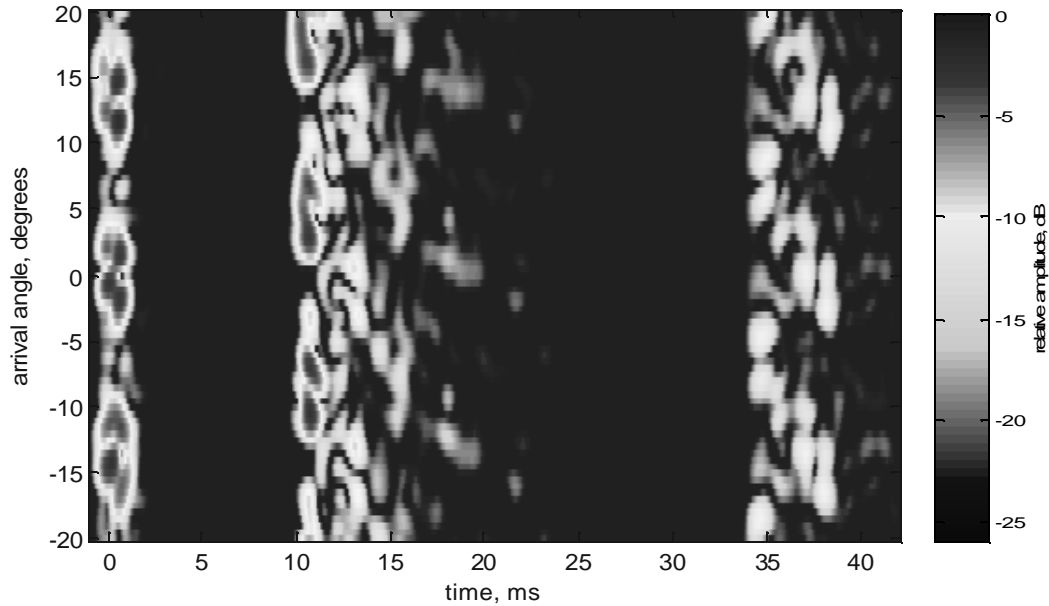
FIGURE 5 - Incoming energy as a function of time and arrival angle for geotime 7/2/04 12:31 (center frequency of energy is 11 kHz and bandwidth is 2 kHz).

The vertical repetition is noticed in the series of arrivals at 0 and 10 msec. From the above formula, the aliasing angle at 11 kHz and 0.6 meter element spacing at which incoming energy will be aliased (for small arrival angles around 0°) is calculated to be 13.2°. We take half of this angle on each side (i.e. 6.6°) for the angular region of analysis.

Based on the above analysis, it is difficult to distinguish the aliased energy peaks from the actual ones. It is possible however to appeal to the known ocean conditions (source depth, receiver depth, and sound speed profile) to eliminate some regions of the arrived energy as being inconsistent with known transmission characteristics. This is a topic of future analyses. In this paper we are concerned with variation from set to set (i.e. 3 second time separations) and from transmission to transmission (i.e. 30 minute time separations). The following plots will concentrate on the angular region from -6.6° to 6.6°, recognizing that energy arriving from larger angles (e.g., via surface interactions) will be aliased.

SIGNAL VARIABILITY

Variability over Long Geotime

To show the effects of ocean variability on the acoustic pulse propagation, two time scales are considered. We refer to these time scales as the short and long geophysical times (abbreviated here as "geotimes") corresponding to the transmission intervals of 3 seconds and 30 minutes respectively. The beamformed time-angle plots shown in Fig. 6 depict the pulse arrivals for four separate geotimes.
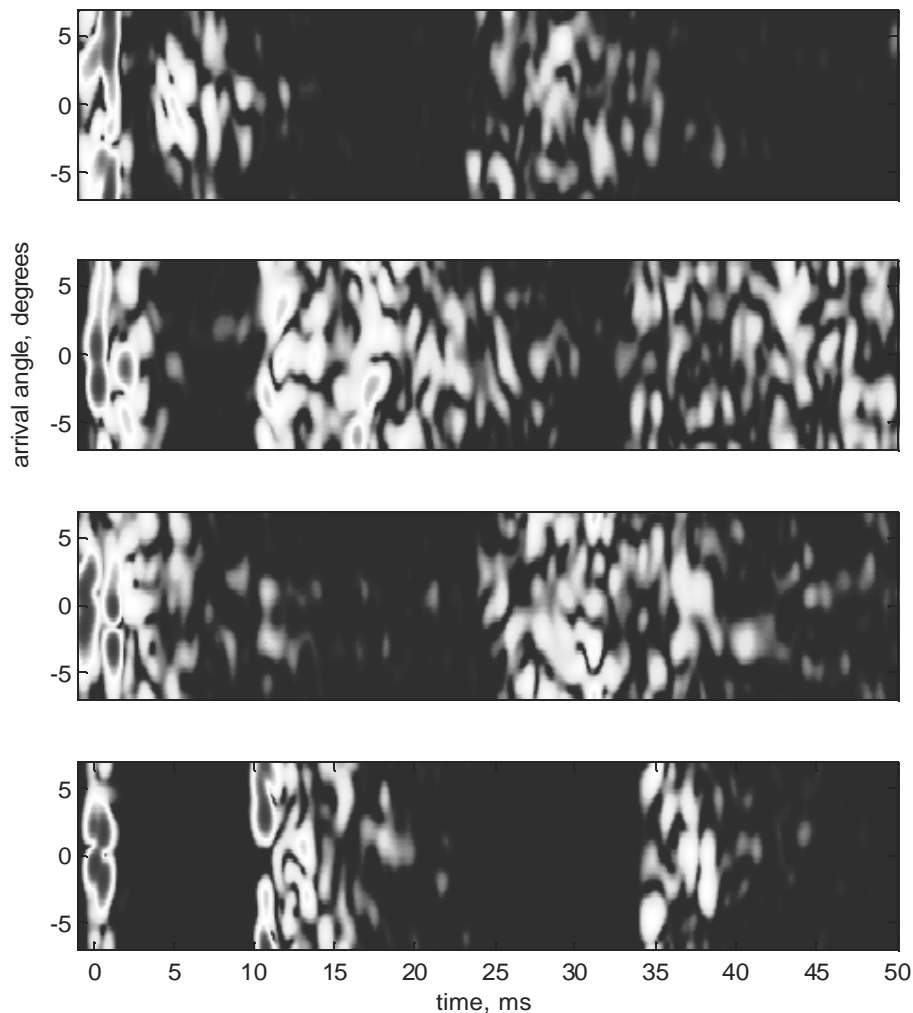
FIGURE 6 - Time-angle plots for showing a large variation in the macro-structure of the ray arrivals over few hours during 7/2/2003. (A) 00:01 AM, (B) 04:01 AM, (C) 06:00 AM, (D) 12:32 PM.

Based on the temperature variations shown in Fig. 2, the sound speed profile over this period changes radically, with the sound speed near the bottom varying by about 10 meters/sec. However, as shown in Fig. 3, the surface is relatively calm over this period.

Variability over Short Geotime

Next the variation of the time-angle fluctuations over signal transmissions separated by 3-second time intervals is considered. An example of short geotime variations of the beamformed results is shown in Fig. 6.
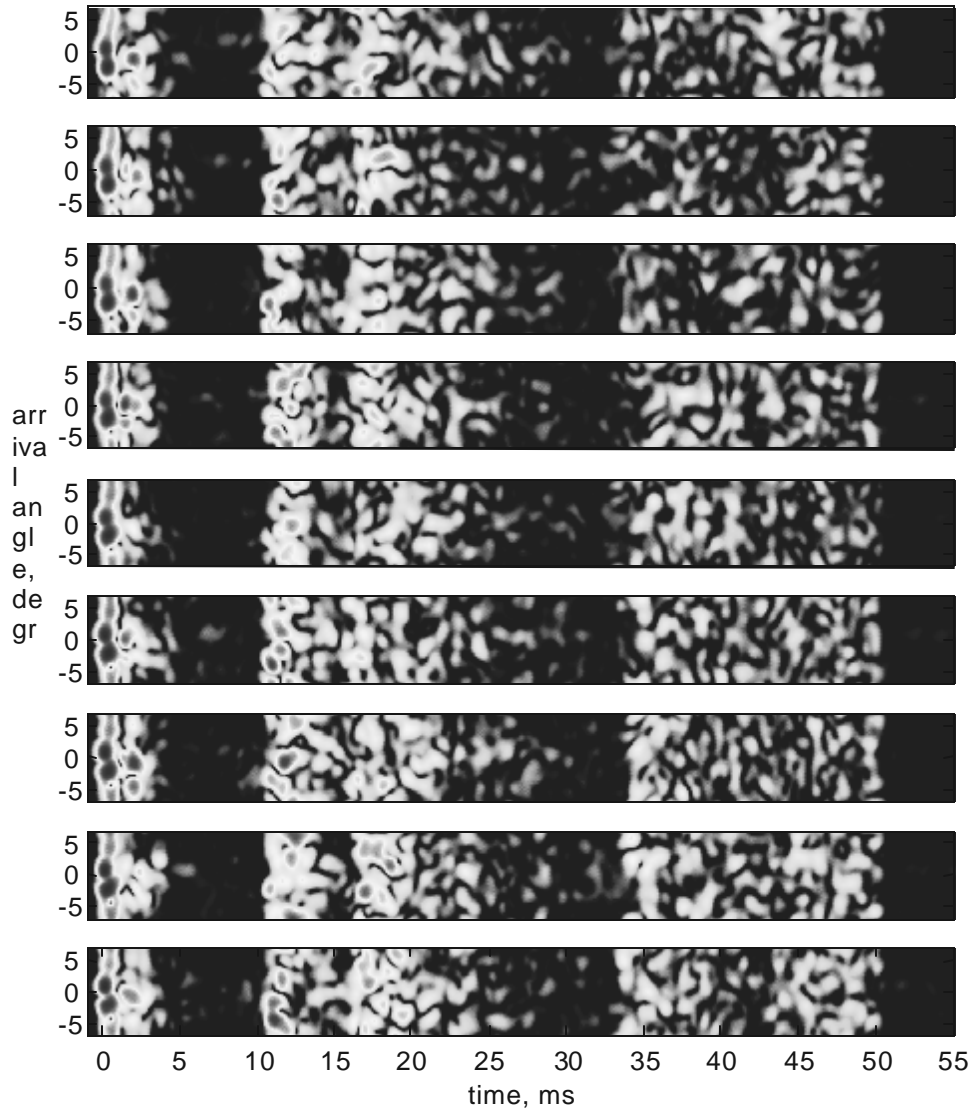
FIGURE 7 - Time-angle plots for 9 transmissions over 27 seconds starting at 7/2 04:01 AM.

At first glance, the frame-to-frame stability of the received signal is noted for the energy arriving from 2-4 msec. The coherence of the first surface arrival (11 msec.) is also noted in Fig. 7. This arrival time corresponds to an almost flat, calm sea surface (Fig. 3 for surface waves and wind conditions at 7/2/2003 around 04:00 AM). The surface-reflected energy is somewhat stable, corresponding to the observed surface wave energy spectrum for this geotime (long period waves, not much chop). It is also noted that the later surface-interacting arrivals (34-50 msec.) are not as coherent as the

earliest arriving energy. To interpret these results, a ray tracing calculation for the experimental source-receiver geometry is shown in Fig. 8.
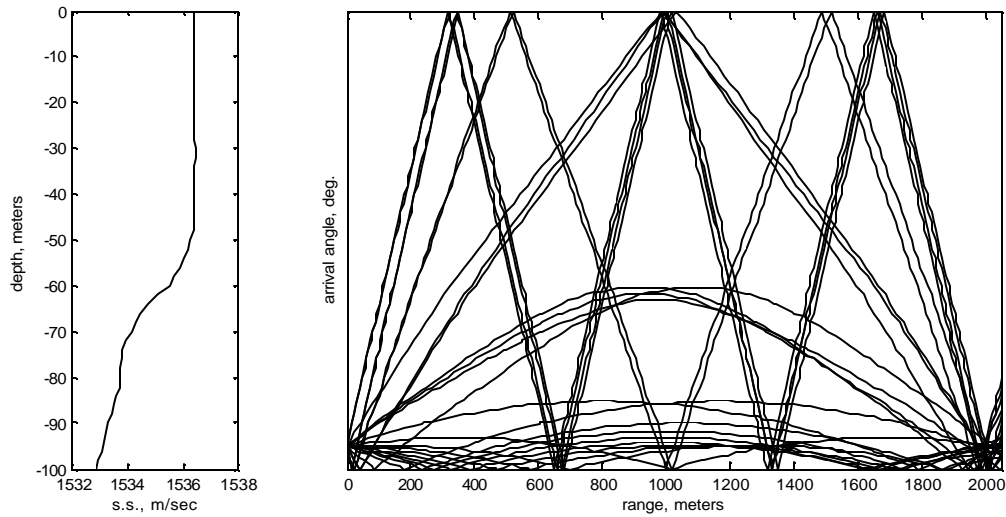
FIGURE 8 - Eigenrays for 07/02/04 04:00 AM showing rays arriving from distributed sources (94-100 meters depth) at 2000 meters range. The receiver is placed at range=0, depth 95 meters.

The number of eigenrays included in this display has been arbitrarily limited by restricting the ray fan emitted from the source. In practice, this limit would be controlled by the bottom critical angle; however, we are only interested in broad qualitative features here. Since the source depth for the experimental data was at 95 m, we consider a range of source depths between 94 and 100 meters and calculate the eigenrays for different depths. The following diagrams in Figs. 9 and 10 show an angular distribution of possible significant eigenrays as a function of arrival time and angle for different combinations of surface and bottom interactions.
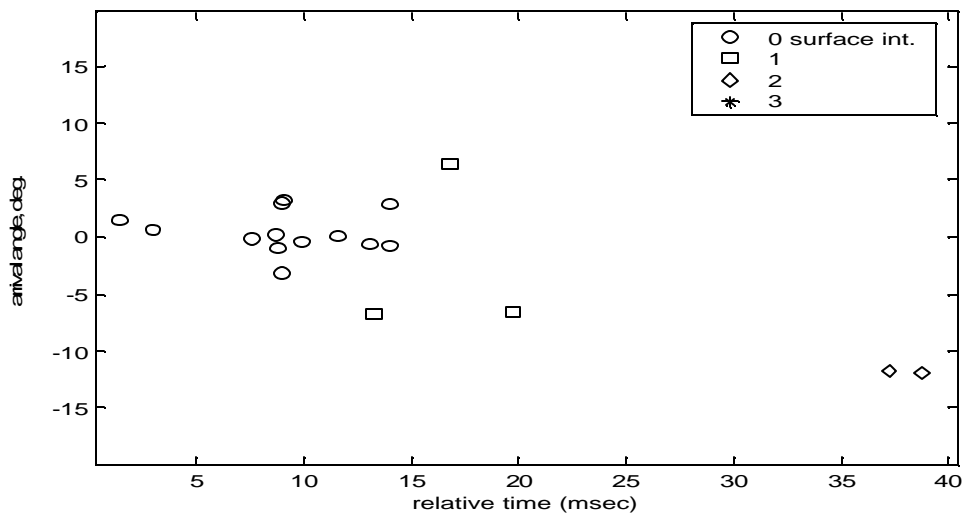
FIGURE 9 - Calculated ray arrival times versus arrival angle showing the number of surface interactions for the sound speed profile on 7/2/2003 at 04:00 AM.
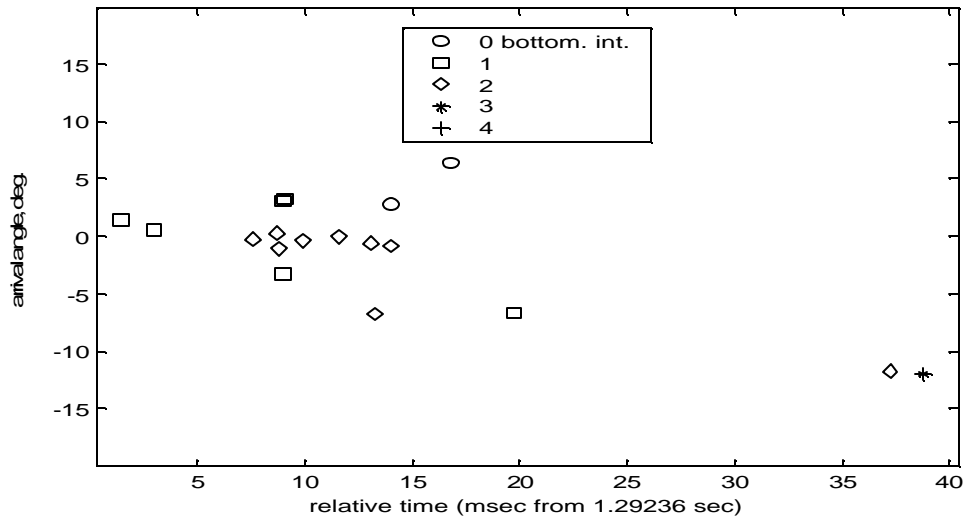
FIGURE 10 - Calculated ray arrival times versus arrival angle showing the number of bottom interactions for the sound speed profile on 7/2/2003 at 04:00 AM.

The spread in time-angle arrivals in these two figures indicates that bottom-interacting energy of the signal could be over a period of about 13 msec. In the set of arrival diagrams shown in Fig. 11 (covering a period of 27 sec) the early arrival shown (i.e. 0 msec.) corresponds to bottom-bounce energy only. The later arrivals are surface interacting. This is known *a priori* from the geometry and sound speed profile at that geotime.

Finally, the effect of rough sea surface is shown in Fig. 12 during 9 transmissions (a period of 27 sec) starting at 7/1 12:31 PM. Note the lower amplitude and the lack of coherence of the surface reflected signals. The energy shown in the plots from 4-10 msec. is bottom interacting, based on the ray tracing calculations. Surface interacting rays are absent. This is due to high-frequency surface waves (the choppy surface shown in Fig. 2) during this period. The low amplitude and lack of coherence in the bottom-interacting signals that arrive around 5 msec. and the signals arriving between 25 to 30 msec. are not fully resolved at this time.

SUMMARY

High-frequency acoustic signals are affected by the small and large spatial and temporal scale variations of the ocean environment processes. These processes can be due to the ocean volume or the dynamic boundary condition roughness. Concurrent oceanographic and acoustic observations were made near a shallow water region of Kauai Island, Hawaii in summer 2003. A subset of the data collected during the experiment is presented here to examine the correlation between the oceanographic variability and the high frequency acoustic wave propagation. Results show a direct relationship between sound speed changes, the surface wave spectrum, and the acoustic wave propagation in this shallow water region.
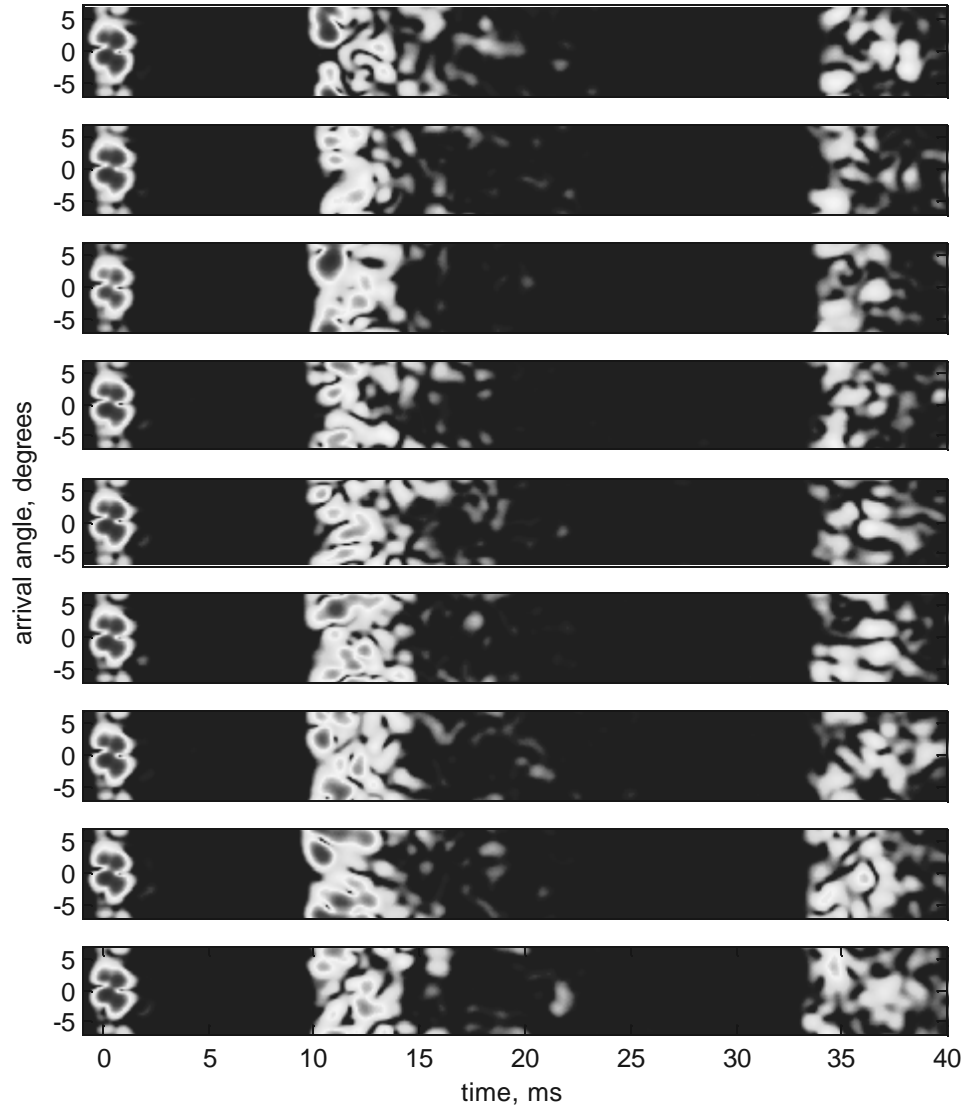
FIGURE 11 - Time/angle arrival picture for geotime 7/2/04 12:32, showing significant arrivals (time scale start is arbitrary, and is set so that t=0 is approximately the time of first arrival).
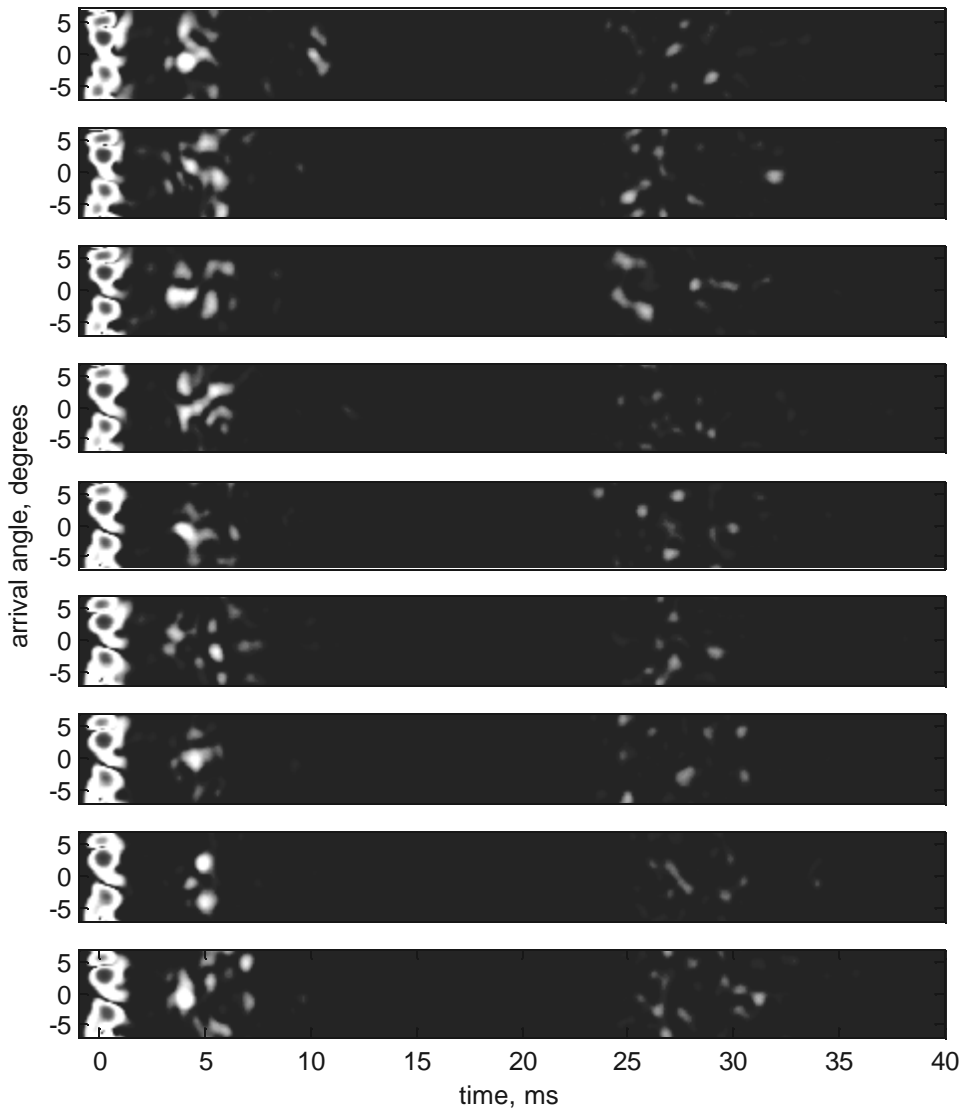
FIGURE 12 - Time-angle plots for 9 transmissions starting at 7/1/04 12:33. Note that during this period the surface was very rough (see Fig. 3).

ACKNOWLEDGMENTS

Sundberg, Luc Lenain, and Robert Heitsenrether (UDel), Paul Hursky, Martin Siderius (SAIC), Jerald Caruthers (USM), William S. Hodgkiss, Kaustubha Raghukumar (SIO), Daniel Rouseff and Warren Fox (APL-UW), Christian de Moustier, Brian Calder, Barbara J. Kraft (UNH), Keyko McDonald (SPAWARSYSCEN), Peter Stein, James K. Lewis, and Subramaniam Rajan (SSI).

REFERENCES

1. Porter, M. B., et al., "The Kauai Experiment," this volume.
2. Badiey, M., Mu, Y., Forsythe, S., Simmen, J., Lenain, L., "*Arrival Time Fluctuations for High-Frequency Pulse Transmissions in Shallow Water*," 5th European Conference on Underwater Acoustics: ECUA2000, France, 2000.
3. Carbone N., and Hodgkiss, W., "Effects of Tidally Driven Temperature Fluctuations on Shallow-Water Acoustic Communications at 18 kHz," *IEEE Jour. Oceanic Engr.*, Vol. 25(1), 2000.
4. Badiey, M., Lenain, L., Wong, K., "*High Frequency Acoustic Propagation in the Presence of Oceanographic Variability*," published in book entitled Impact of Littoral Environmental Variability on Acoustic Predictions and Sonar Performance, edited by N. Pace and F. Jensen, Kluwer Academic Publishers, pp.35-42, 2002.